Oil Film Characterization of PTFE During EHL Point Contact and Pure Rolling Tribology Tests

2021 IEEE 8th International Conference on Adaptive Science and Technology (ICAST) | 978-1-6654-2717-3/21/$31.00 ©2021 IEEE | DOI: 10.1109/ICAST52759.2021.9681972

Glenn Kwabena GYIMAH
Accra Technical University,
Department of Mechanical Engineering,
Accra, Ghana.
gkgyimah@atu.edu.gh

Shuzhen JIANG
Lingnan Normal University,
School of Mechanical and Electronic Engineering, Zhanjiang, P.R. China.
szjiang@lingnan.edu.cn

Amevi ACAKPOVI
Accra Technical University,
Electrical/Electronic Engineering Department, Accra, Ghana.
acakpovia@gmail.com

Emmanuel Kabu OMAN
Accra Technical University,
Department of Mechanical Engineering,
Accra, Ghana.
ekoman@atu.edu.gh

Peter NYANOR
Accra Technical University,
Department of Mechanical Engineering,
Accra, Ghana.
pnyanor@atu.edu.gh

Gary C. BARBER
Department of Mechanical Engineering,
Automotive Tribology Center, Oakland University, Rochester, MI, U.S.A.
barber@oakland edu

Abstract— A polymer additive blended with commercial engine oil to have enhanced film-forming ability has been developed and studied using optical interferometry. An experimental study was carried out on the impact of polymer additives (Polytetrafluoroethylene – PTFE) in an oil film between a steel ball and a flat glass surface in non-conformal contact. The contact region was studied by means of optical interferometry using monochromatic two-beam interferometry, a microscope and a high-speed video recording device. A new method of determining the interference grade of the central film thickness was developed and used in this study. The interference intensities of the central point of contact at various speeds were captured by the high-speed video recording device and the central interference gray values were determined. These values were then used in new method to obtain the film thickness of the modeled lubricants, and compared with the rectangular SLIM fit and the LINE fit methods film thickness determination. Hamrock and Dawson calculations for EHL film thickness formation was also used for comparative analysis. The film thickness stability was simulated under both steady state and rolling state conditions. The lubricant film thickness stability obtained confirmed the beneficial effect of PTFE on film thickness behavior under pure rolling conditions. The regime observed by the profile of the film thickness suggest the transition between the hydrodynamics and elastohydrodynamic lubrication.

Keywords: EHL lubrication; Contact pressure; Film thickness; Rolling contact speed; Pure Rolling.

Nomenclature

u : the flow velocity in the x direction respectively
h : is the film thickness
h_1 : is the minimum film thickness
U : is the sliding velocity of the solid surface
l : is the characteristic length of micro-polar fluid
L : is the dimensionless characteristic length
N : is the coupling coefficient
μ : is the Newtonian fluid viscosity
χ : is the rotational viscosity of the micro-polar fluid
ρ : is the density
P : pressure
f : dimensionless stream function
υ_s : micro rotation/spin-gradient viscosity

I. INTRODUCTION

The study of lubrication together with that of friction and wear forms, which is known as tribology, is the science and technology that deals with contacting surfaces in relative motion. Those phenomena occur in the contact of many machine components. Examples of applications in which tribology plays an important role include gears, cam and follower mechanisms, traction systems, brakes, bearings, cutting tools and clutches. The performance of the components involves many variables such as tribological conditions, materials and surface conditions, and environment [1]. In Figure 1 a schematic representation of the tribo system is presented. It is composed of two bodies in

978-1-6654-2717-3/21/$31.00 ©2021 IEEE

contact (1 and 2), with a lubricant (3) in between and operating in a certain environment (4). In view of the high given operating conditions and structural parameters, the tribo system generated contact stress or deformation, friction, heat, and wear. In order to deal with the characteristics of a tribo system, one vital element to consider is the lubricant used in the system between the tribological contacts. Admittedly, lots of effort have been made to understand the influence of these variables including lubricants and the interaction between them, and that has resulted in the optimized performance of machine elements.

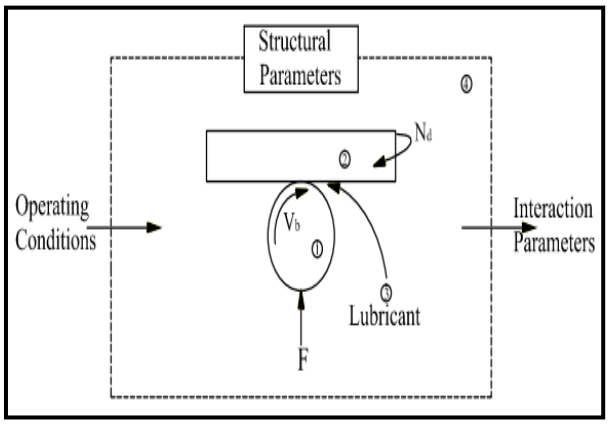

Figure 1 A schematic Diagram of the Tribo-system [2]

Nevertheless, much work on the appropriate lubricants to be used for a system, in order to withstand the conditions likely to be encountered, has always been the problem. The choice of lubrication oil in the tribological system, cost, as well as impact on health, safety and the environment factors are key issues to be considered in the selection of the lubricant. The properties of these oil lubricants are very vital to the tribological system. Basically, these properties depend on the base oil (or blends of the base oils) and on the improvers additives used.

The presence of polymers represent an important category of improvers additives incorporated into the base oils, increasing the viscosity and therefore the lubricant film thickness [2-9]. Polymer-thickened lubricants have been in use as far back as the 1950s to increase the viscosity and lubricant film thickness [10 - 12]. The performance of engine oil with mixed polymers as lubricant additives, e.g., they have combined properties of poly (alkyl methacrylates) with olefin copolymers and hydrogenated styrene-diene copolymers, was investigated by Omneis et al. [13]. The role of the molecular weight distribution in the polymer, influencing the lubrication of the machine element, was put forward by Hirano and Larsson et al. [14,15]. Introducing polymer additives of wide molecular weight distribution into engine oils, have resulted in a longer life for rolling bearings, compared with oils with polymer additives with narrow molecular weight distribution. At very low speed, absorbed polymer layers, with a viscosity higher than those of the bulk solution in the film thickness formation, have been obtained by Martini, Smeeth, and Gunsel [15-17]. The authors used the evidence observed, to define the properties of an elastohydrodynamic film in the boundary lubrication regime, because, viscous boundary layers were able to generate elastohydrodynamic - type of films. Spikes and Guegan [19,20] investigated and explained the formation of the film thickness properties of polymer additives solutions, base oil with ciscis polyisoprene, in the elastohydrodynamic lubrication of a concentrated rolling ball on disk point contact. The technique adopted for the analysis was the optical interferometry method, they have evidenced the effect of very viscous layers (up to 17 nm thick) formed by the polymer adsorption. Spike and Guegan [18, 20] asserted that, the optical interferometric methods are well established and routinely used to obtain lubricant film thickness and profile shape data. Presently, engineers are faced with increasing demands of less expensive, more efficient, and environmentally friendly lubricants, which will prolong machine elements such as gears, bearings, rollers, cams and the rest. Thinner lubricating films are often used e.g., Dowson [21]; thus, the surface topography becomes very important in the life cycle of the machine elements in contact. Until now, there have been many types of solid, liquid and composite lubricant materials that have been used in the automobile industry. The solid lubrication materials mainly included polymer, graphite, copper alloy, MoS_2 composite materials, soft metal coatings (Ag, Au, Pb, In) and diamond-like carbon (DLC), and so on [22–25]. The solid–liquid lubricating materials could be designed and validated to improve service reliability and extend the life of the mechanical rolling elements, which have attracted extensive research interest recently. In this research work, polymer material was considered due to its attractiveness in broad application domains and its particular properties, such as self-lubrication properties, low weight, excellent mechanical properties, easy manufacturing processes, high wear resistance, radiation stability, outstanding thermal stability and admirable chemical stability [26–28]. The kind of polymer additives used was polytetrafluoroethylene (PTFE). This is because it is a common solid lubricating material and widely applied in bearings and seals [29]. Therefore, PTFE could act as the admirable candidate substrate element for new types of solid–liquid lubricating materials. The regime in which this research work was studied is elastohydrodynamic lubrication (EHL), and it is found in contact elements such as, rolling element, bearings and gears [30]. These contacts are non-conformal contacts therefore, such elements are subjected to very high contact pressures (in the gigapascal region) and elastic deformation which has become an issue of great concern. The film thickness profile of the lubricant generated from the EHL will be used to predict the form of lubrication

regime and film thickness stability (the ability to separate and sustain surfaces) under different operating conditions.

II. EXPERIMENTAL PROCEDURES AND MATERIALS

2.1 Lubricant Formulation

This study required commercially available sample of polymer (PTFE) powder and a commercially available super refined engine mineral oil as the base and reference oil (SAE #30). These lubricants (liquid and solid) were blended together to obtain a modeled lubricant. The concentration of PTFE was selected for the experimental studies: 5.0 % (12.5g PTFE powder of 1µm size), in volume grams of polymer dispersed into 250 mL of SAE #30 engine oil. The additivation of mineral oil with polymer was realized by mixing the polymer solid particles with the base oil under continuous stirring at 21ºC. The temperature for this study was within 20ºC to 21ºC. All the two lubricants used and their properties are listed in Table 1. In Figure 2 is the picture of the modeled polymer solutions and base lubricant that were tested in their measured proportion in volume weight. Viscosity values were obtained by using a rheometer with rotary cylinders as tabulated in Table 1. The densities were measured by ASTM D 1298 at temperature 21°C. The refractive indices of the sample models were measured using an Abbe refractometer. For more details of the experimental procedure, refer to the work [2].

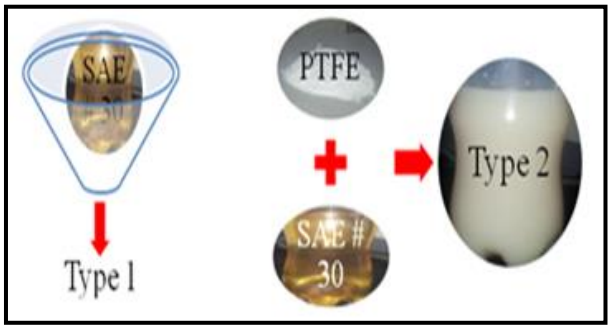

Figure 2 Shows the concentrations of the base lubricants (100% SAE # 30), type 1, and type 2, 5% (12.5g PTFE+250mL base of SAE #30)

2.2.1 Viscosity – Temperature Relation

Most lubricant viscosities drastically decline with increase in temperature. In this investigation, the Vogel relationship was used due to the degree of accuracy that it guarantees:

Vogel

$$\eta = ae^{\frac{b}{(T-c)}} \quad (1)$$

Where, η represents the absolute viscosity (cP) at reference temperature T (ºC) (often at the film inlet) and *a*, *b*, *c* are constant.

2.2 Description of the ROII Technique for Measuring Lubricant Film Thickness

This technique is fully described in detail in reference [31], and the equation to resolve the film thickness formation is expressed as.

$$h = \frac{\lambda}{4\pi k}\left\{n\pi + \left[\arccos\left(\bar{I}\right) - \arccos\left(\bar{I}_0\right)\right]\cdot\cos n\pi\right\} \quad (2)$$

where *n* is the interference grade, $n = 0, 1, 2\ldots\ldots$ $\bar{I}$ is the relative grey value; $\overline{I_0}$ is the relative grey value where the film thickness is 0; λ is the wavelength of the light; *k* is the refractive index of the lubricant. In a practical method for the relative gray value, $\bar{I}$ and $\bar{I}_o$, in the case where the film thickness is 0, the following formula is used to obtain the relative grey value.

$$\bar{I} = \frac{2I - \left(I_{\max} + I_{\min}\right)}{I_{\max} - I_{\min}} \quad (3)$$

Furthermore, Equation 2 generated less smooth film thickness distribution, due to less accuracy of the equation for every interference grade, particularly when the interference grade is an odd number. Therefore the following modification was arrived at for interference grade (*n*) of odd numbers.

$$h = \frac{\lambda}{4\pi k}\left\{(n+1)\pi + \left[\arccos\left(\bar{I}\right) - \arccos\left(\bar{I}_0\right)\right]\cdot\cos n\pi\right\} \quad (4)$$

When the grades (n) are even numbers, the following is used:

$$h = \frac{\lambda}{4\pi k}\left\{n\pi + \left[\arccos\left(\bar{I}\right) - \arccos\left(\bar{I}_0\right)\right]\cdot\cos n\pi\right\} \quad (5)$$

Therefore, the film thickness calculation was generated from the grey values distribution obtained from the interferogram and used in the Equation 4 and 5.

2.2.1 Experimental Apparatus Status and Methods

The optical film interferometry technique employed to measure lubricant film thickness formation in a rolling ball-on-flat contact which was originally described by Luo et al. [32-34] was used. The full view of the optical interferometry film thickness in EHL point contact apparatus setup used, is shown in Figure 3. The Hertz pressure contact area is formed between the steel ball and the flat surface of the glass disc under fully flooded EHL condition. A beam of light of wavelength of 600 nm reaches the contact surface of the Cr layer. It is divided into two beams, and one is reflected from the upper surface chromium layer whiles the other goes through the Cr layer and the lubricant film present to be

reflected at the surface of the steel ball. These two beams recombine and they become interference lights. At zero incident angle, the optical interference equation [35] is as follows.

$$I = I_1 + I_2 + 2\sqrt{I_1 + I_2}\cos\left(\frac{4nh\pi}{\lambda} + \phi\right) \quad (6)$$

where I is the intensity of the interference light at the point where the lubricant film thickness h is to be measured, I_1 is the intensity of beam 1 and I_2 is that of beam 2, λ is the wavelength of the light after the monochromator, ϕ is the phase change caused by the Cr layer and the steel ball, and n is the oil refractive index. The interfered light is then passed through the microscope into a spectrometer where it is dispersed and detected by the CCD camera which captures the interfered images within the frame range. The interfered images are finally sent to the computer to be displayed. Spinning of the steel ball is an issue, therefore, the rotational axis of the ball is directed towards the surface at the center of the disk. In the work described in this study, the disc was rotated and drove the ball itself in nominally pure rolling. A new 25.4 mm diameter steel ball of 3.5 nm surface finished of RMS roughness was used for each test. The disk (152.4mm in diameter) was of a surface finished of RMS roughness σ = 5 nm. The loads applied were 1N and 2N which corresponded to a Hertz maximum contact pressure of 0.1635 GPa and 0.2047 GPa. The linear velocities were 0.189m/s, 0.382m/s and 0.641m/s. The rotational speeds of the disk, the load that is applied on the rolling elements, and the distance of the contact with respect to the center of the disk, can all be adjusted to any experimental design.

Figure 3 The setup of the optical interferometry image capturing.

2.2.3 Experimental Conditions

The experiments were conducted at the temperature, contact pressures and rolling speeds given in the Table 1.

Table 1. Experimental Testing Conditions

Testing Condition			
Contact Loads (N)	1 – 2		
Maximum Hertz Pressure GPa	0.162, 0.186, 0.205, 0.223		
Rolling Speed (m/s)	0.189, 0.383, 0.641		
Temperature (°C)	21		
Ball Diameter	25.4mm (σ=3.5)		
Disc Diameter	152.4mm (σ=5 nm)		
Tested Lubricants Properties			
Lubricant Type	Ref Index	Viscosity	Density
T_1（100%SAE #30 oil)	1.5	0.205 Pa.s	890 kg/m^3
T_2 (5%PTFE+SAE #30）	1.478	0.255 Pa.s	892 kg/m^3

2.2.4 Interference Images

For the procedure used in order to measure the film thickness with minimum error, it is necessary to obtain interference fringes from a lubricated steel ball on coated glass surface, as illustrated in Figure 4. The quality of the fringes and the degree of accuracy of the measurements taken with the interferometer, primarily depend on three conditions of the reflecting surfaces. The very immediate and important is the surface finish. Therefore, proper care must be ensured to satisfy this by obtaining optically smooth surfaces for both the glass and the steel ball. The second condition concerns that of geometric values. It is necessary to obtain a meaningful measurement of elastic deformation and it is essential that the initial deviation from a perfect surface geometry is small in comparison with the deformation due to pressure. This is primarily the reason for limiting this experiment presented to a point contact. The third condition is that of reflectivity. In monochromatic interferometry, fringes of high visibility are obtained if the intensities of the two beams are equal ($I_1 = I_2$), and this is achieved by controlling the reflectivity of the surfaces. It is possible to obtain fringes of good visibility with very low reflectivity, although this is an inefficient use of the total light input. It is this feature of two-beam interferometry that makes film thickness measurements of surfaces with low reflectivity possible. To obtain fringes of high visibility, it is extremely important that the reflectivity of the optical window is comparable with that of the steel ball, to make the intensities of the two interfering rays approximately equal ($I_1 \approx I_2$). A series of cropped were done after an image-intensifying camera was used to capture the interferograms. The speeds used for the interferograms are 30rpm, 61rpm and 102rpm for fixed loads of 1N, and 2N with two different lubricants (SAE #30 mechanical oil) and (SAE #30 mechanical oil with 5% PTFE additives). Lubricant flows along the X plane from left to right. The location of the minimum film thickness may occur at the center line, or at the side lobes [36 - 39]. But in this work, the monochromatic system shows good detail in

film shape and it can be seen that for all the images, the minimum film thickness occurs at the lubricant outlet constriction.

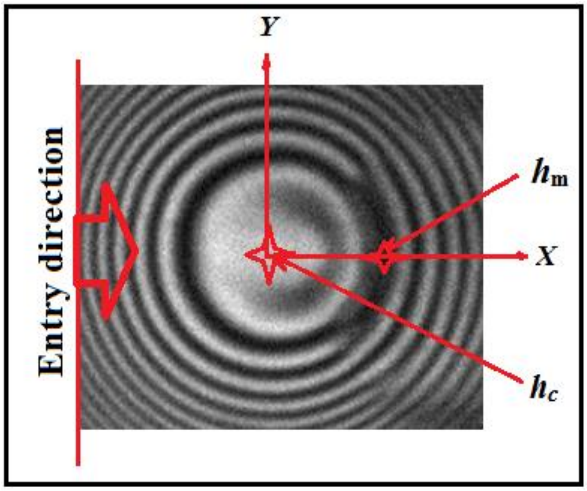

Figure 4 Dynamic intensity interferogram

2.3 Numerical Method

The minimum thickness of the lubricating film separating the surfaces in an EHL contact, is of primary interest to a design engineer concerned with such contacts. The successful separation of the surfaces under the anticipated operating conditions, can significantly increase the useful life of the machine parts involved. If separated, the failure mode will be the long term limitation of surface fatigue. If the surfaces are not separated adequately, surface interaction will shorten the contact life and may even result in sudden scuffing failure.

The purpose of this section was to determine numerically by using the Hamrock and Dowson (1981) formula, the minimum and central film thickness as a function of rolling velocity, normal load, and contact geometry in a fully flooded EHL point contact in pure rolling of the novel blended lubricants (T_2) and compare it with the standard SAE #30 mechanical lubricant (T_1). The Hamrock and Dowson (HD) film thickness equation.

For central film thickness

$$\frac{h_c}{R_x} = 2.69\left(\frac{U\eta_0}{E'R_x}\right)^{0.67}(\alpha E')^{0.53}\left(\frac{W}{E'R_x^2}\right)^{-0.067}\left(1-0.61e^{-0.73k}\right) \quad (7)$$

$$\frac{h_c}{R_x} = 2.69U^{0.67}G^{0.53}W^{-0.067}\left(1-0.61e^{-0.73k}\right) \quad (8)$$

For minimum film thickness

$$\frac{h_m}{R_x} = 3.63\left(\frac{U\eta_0}{E'R_x}\right)^{0.68}(\alpha E')^{0.49}\left(\frac{W}{E'R_x^2}\right)^{-0.073}\left(1-e^{-0.68k}\right) \quad (9)$$

$$\frac{h_m}{R_x} = 3.63U^{0.68}G^{0.49}W^{-0.073}\left(1-e^{-0.68k}\right) \quad (10)$$

Hamrock and Dowson [40-43] only intend this equation to be used for ellipticity ratios greater than one or equal to one ($k \geq 1$) and it is speculation on the authors' part that it is valid for ellipticity ratios less than one ($k < 1$). Based on our research work, the experimental procedure adopted a pure rolling point contact, which uses (k=1) and is justified by the authors.' k=1 for pure rolling point contact. In this section, EHL minimum and central film thickness measurements were obtained at various levels of dimensionless speed and load. The dimensionless material parameter was maintained at a constant. The dependent variable, dimensionless film thickness, was obtained for each set of independent variables: speed, and load, and the results will help predict the lubrication regime. Table 2 presents the experimental parameters of the machine, the steel ball, the disc and the lubricants.

Table 2 Representative Experimental Parameters

Glass disc diameter	0.065 m	Elastic modulus of glass	7.60 x 10^{10} Pa
Steel ball diameter	0.0254m	Poisson ratio for glass	0.25
Steel ball radius	0.0127m	Elastic modulus of steel	2.10x 10^{11}Pa
Radius parameter R	0.0127m	Poisson ratio for steel	0.28
Optical index (SAE #30)	1.5	E', the reduced E	1.20 x 10^{11}Pa
Optical index (SAE+PTFE)	1.478	Wavelength	450-850nm
Phase shift	0.1		

In the experimental setup used, a ball is in contact with a flat surface. In the next section a case is considered in which an elastic ball is in contact with a rigid half space.

2.4 Theoretical Method

2.4.1 Film thickness

For the point contact solution, the area is generally rectangular in shape as illustrated in Figure 5, where AB and CD are the inlet and outlet borders respectively. The leakage sides are the AD and BC. The solution domain could be seen in the figure as with the symbols, α, β and γ.

The film thickness under elastic deformation can be expressed as follows.

$$h(x,y) = h_0 + \frac{x^2}{2R_x} + \frac{y^2}{2R_y} + v(x,y) \quad (11)$$

where, h_0 is the center film thickness to be determined in calculation; R_x and R_y are the equivalent curvature radii in the x and y direction; and $v(x,y)$ is the elastic deformation.

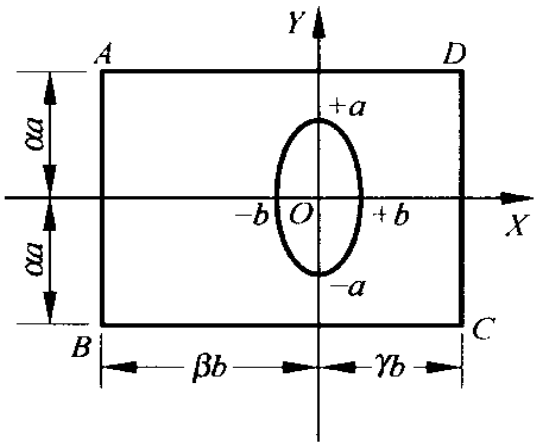

Figure 5 Point Contact: Solution region. [31]

2.4.2 Elastic deformation

The theory of elasticity indicates that, the relationship between the pressure $p(x,y)$ and the deformation $v(x,y)$ can be expressed as follow.

$$v(x,y) = \frac{2}{\pi E}\iint_{\Omega} \frac{p(s,t)}{\sqrt{(x-s)^2 + (y-t)^2}} dsdt \quad (12)$$

where, s and t are the additional coordinates in the x and y directions; Ω is the solving domain; and E is the equivalent elastic module of the surfaces.

Equation 11, further resolutions by transforming the coordinate origin and using polar coordinates will become the following integral equation.

$$v(x,y) = \frac{2}{\pi E}\iint_{\Omega} p''(r,\theta) dr d\theta \quad (13)$$

2.4.3 Pressure distribution and Film thickness of Lubricant

The deformation matrix method is adopted over the numerical calculation which requires a large amount of computation and the numerical integration method also needs a large number of computer storage units. The discrete form of the elastic deformation equation becomes.

$$v_{kl} = \frac{2}{\pi E}\sum_{i=1}^{n}\sum_{j=1}^{m} D_{ij}^{kl} p_{ij} \quad (14)$$

where, V_{kl} is the elastic deformation at Node (k,l) ; p_{ij} is the pressure at Node (i,j); and D_{ij}^{kl} is the elastic deformation coefficient between Node (k,l) and Node (i,j). To reduce computational time significantly with no significant loss of accuracy, substitute D_{ij}^{kl} into Equation 18 to calculate the elastic deformation repeatedly in the iteration process. By the isometric grid mesh, we have

$$D_{ij}^{kl} = D_{kj}^{il}$$
$$D_{ij}^{kl} = D_{il}^{kj} \quad (15)$$

Furthermore, the storage unit can be reduced from $m^2 \times n^2$ to $m \times n$ and the specific formula of the elastic deformation becomes.

$$v_{ij} = \Delta x^2 \sum_{k=1}^{N}\sum_{l=1}^{N} a_{i-k,j-l} p_{kl} \quad (16)$$

The Hertzian contact pressure distribution was used in calculating the elastic deformation of a ball with a radius R contacting with a rigid plane.

III. RESULTS DISCUSSION

3.1 Experimental and Numerical Results

The FULLY flooded EHL dynamic monochromatic interferogram evaluation procedure for this particular research has been illustrated in Figure 4 as labeled. The main features of interest are the h_m and h_c. The experimental results of the film thickness distribution as function of sample lubricant (T_1, and T_2), load and speed at point contact was discussed. The film thickness, was related to the behavior of the grey value. The grey value behavior firmly confirms and agrees with the film thickness of the lubricants. The experiment was centered on two main conditions which are: the steady contact condition and the pure rolling contact condition. In each condition, the film thickness stability as function of load, improving additives, and the contact state as stationary or rolling, was investigated. These are analyzed based on two adapted modes such as, the horizontal '*LINE*' mode and the rectangular '*SLIM*' mode. The two modes were compared to ascertain the true behavior of the film thickness. The experimental ROII technique results by Optical interferometry was also compared with the Hamrock and Dawson numerical formula as a function of the lubricant sample. In Figure 6, the blue squares area selected on all the two samples, T_1 and T_2 are the area of focus (AOF).

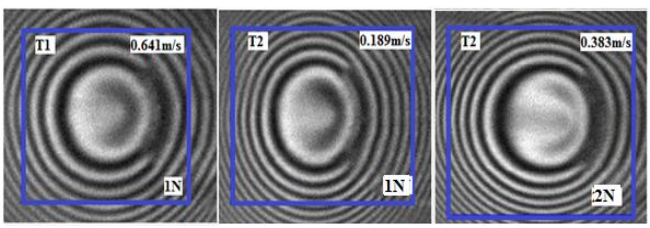

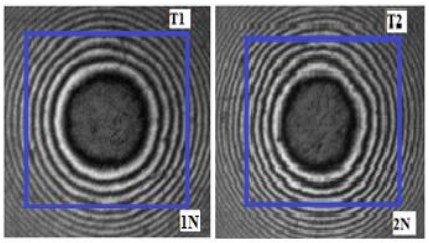

Figures 6 Dynamic monochromatic interferogram AOF for selected lubricants under a stationary and pure rolling condition.

3.1.1 Experimental Film Thickness Distribution – Steady Contact

For the experimental discussion on the tested lubricant at stationary contact; that means at 0m/s speed, the focus was the stability of the film thickness. The effect of temperature on this film is virtually zero. Figures 7 and 8 show the film thickness stability of the two lubricants. The graphs of horizontal line of all the two lubricants at all loads, conformed to the light intensity variation as a cosine curve [44]. The viscosity of the lubricants affected the film thickness due to the load variation. The load weakens the film thickness stability at high loads. But with the inclusion of a lubricant improver such as the PTFE gave firm film thickness stability and supported the high loads. Considering the *SLIM* shape film thickness behavior in Figure 7 and 8, there is consistent stability under the stationary condition. The density of the blended lubricants also contributed to the stability of the film thickness. The last factor that influences the nature of the film thickness is the poor ball surface finish and reflectivity. Interestingly, all the three samples demonstrated film thickness in consistency at the variation found between 0 to 250. More so, there is even distribution of the film thickness, which predicts that the load capacities are very high.

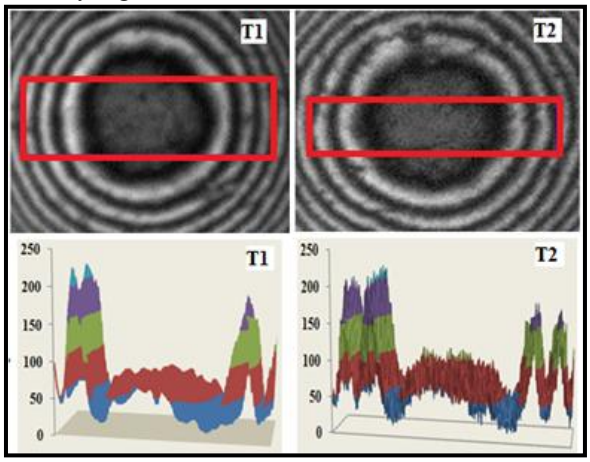

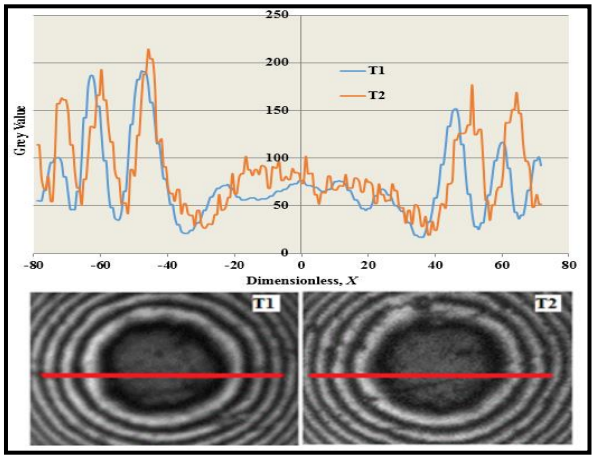

Figure 7 Interferometric images of lubricants film distribution of an EHL point contact operating. *Horizontal 'LINE' and Rectangular 'SLIM' mode*. Parameters: L=1N, T=21°C, P_h=0.162GPa, η for T_1 = 0.205Pa.s, and η for T_2=0.255Pa.s.

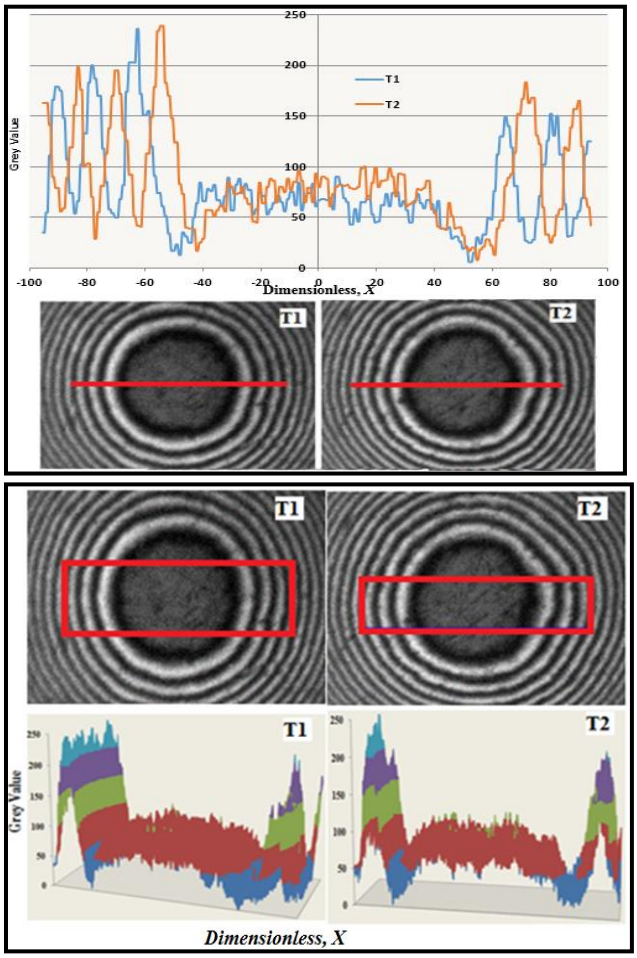

Figure 8 Interferometric images of lubricants film distribution of an EHL point contact operating. *Horizontal 'LINE' and Rectangular 'SLIM' mode*. Parameters: L=2N, T=21°C. η for T_1 = 0.205Pa.s, η for T_2=0.255Pa.s and P_h=0.205GPa.

3.1.2 Experimental Film Thickness Distribution - Pure

Rolling Contacts

The pure rolling here means there is no slippage or sliding. The Figures 9-14 presents the images captured in a pure rolling condition for all the two samples and were analyzed by the use of the horizontal *'LINE'* and rectangular *'SLIM'* section of the area of interest. The optical EHL film thickness stability measured was a function of speed, load, and the improvers' additives. The image quality needed to measure the film thickness was influenced by the surface precision of the steel and the ball. The pictures were at the loads (1N and 2N) and the speeds (0.189m/s, 0.383m/s and 0.641m/s). The results observed under the EHL fully flooded condition shows the transition between hydrodynamic lubrication and EHL regime [45].

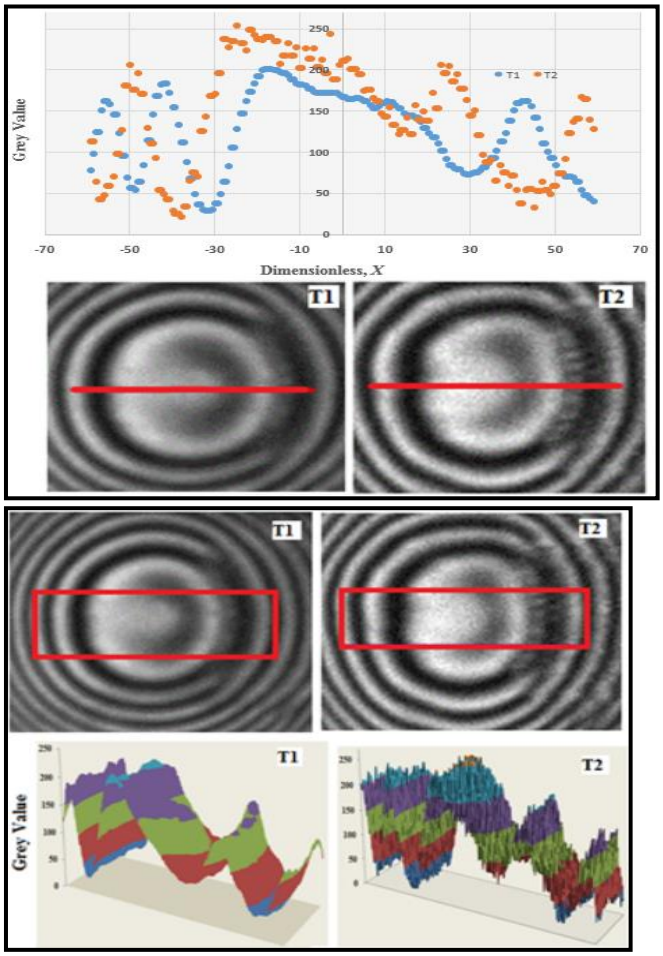

Figure 9 Interferometric images of lubricants film distribution of an EHL point contact operating. *Horizontal 'LINE' and Rectangular 'SLIM' mode.* Parameters: L=1N, U=0.188m/s, T=21°C, P_h=0.162GPa, η for T_1=0.205Pa.s and η for T_2=0.255Pa.s.

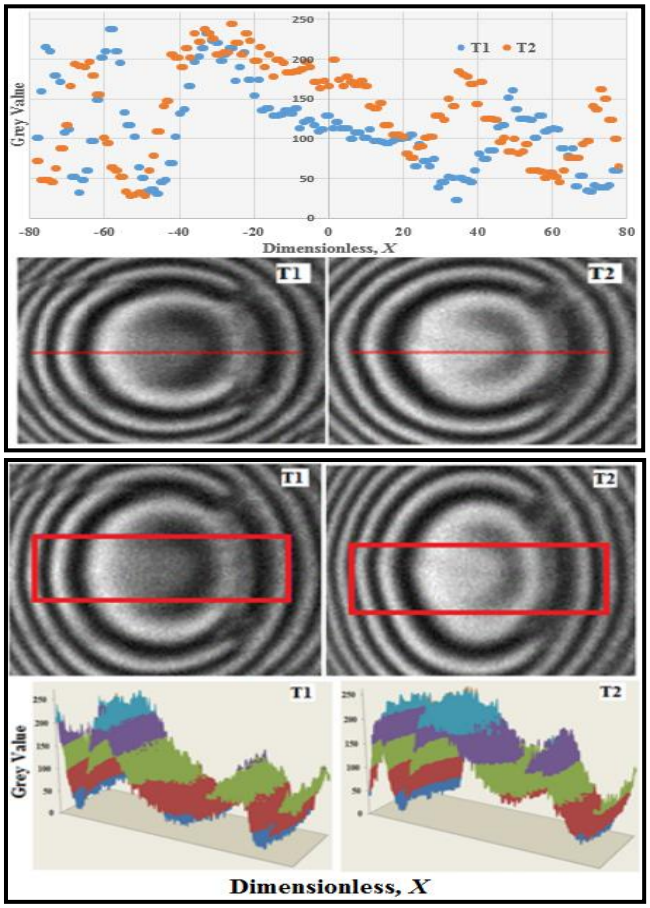

Figure 10 Interferometric images of lubricants film distribution of an EHL point contact operating. *Horizontal 'LINE' and Rectangular 'SLIM' mode.* Parameters: L=1N, U=0.383m/s, T=21°C, P_h=0.162GPa, η for T_1=0.205Pa.s and η for T_2=0.255Pa.s.

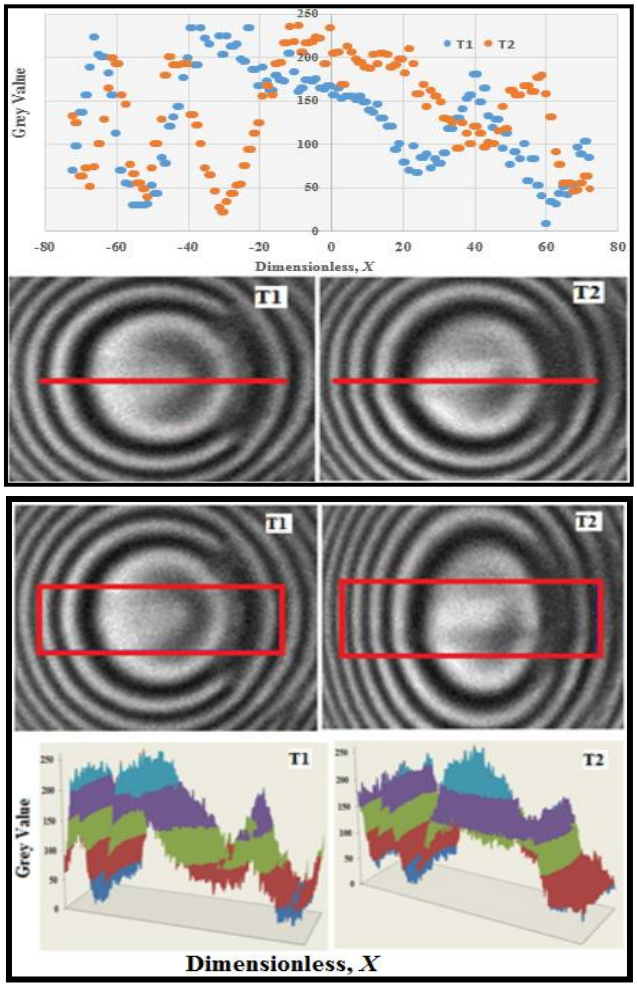

Figure 11 Interferometric images of lubricants film distribution of an EHL point contact operating. *Horizontal 'LINE' and Rectangular 'SLIM' mode.* Parameters: L=1N, U=0.641m/s, T=21°C, P_h=0.641GPa, η for T_1 = 0.205Pa.s and η for T_2=0.255Pa.s.

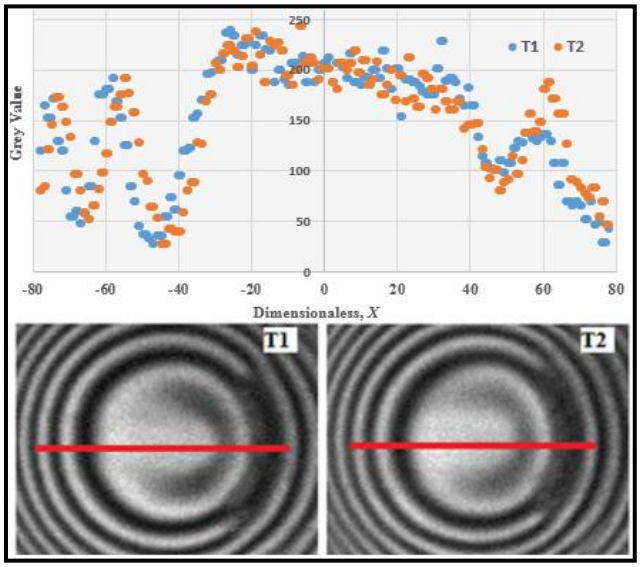

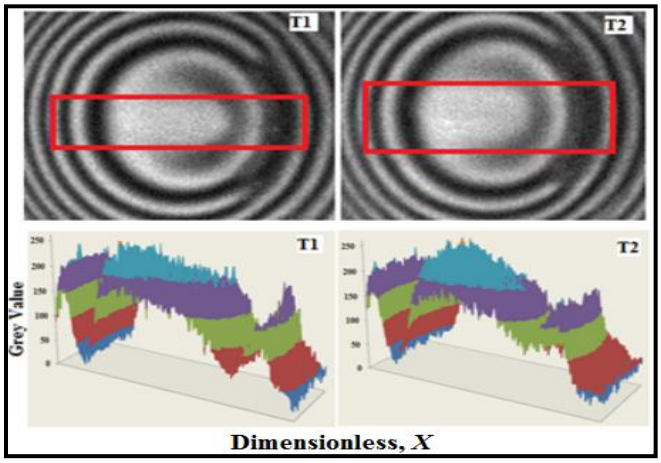

Figure 12 Interferometric images of lubricants film distribution of an EHL point contact operating. *Horizontal 'LINE' and Rectangular 'SLIM' mode.* Parameters: L=2N, U=0.188m/s, T=21°C, P_h=0.205GPa, η for T_1=0.205Pa.s and η for T_2=0.255Pa.s.

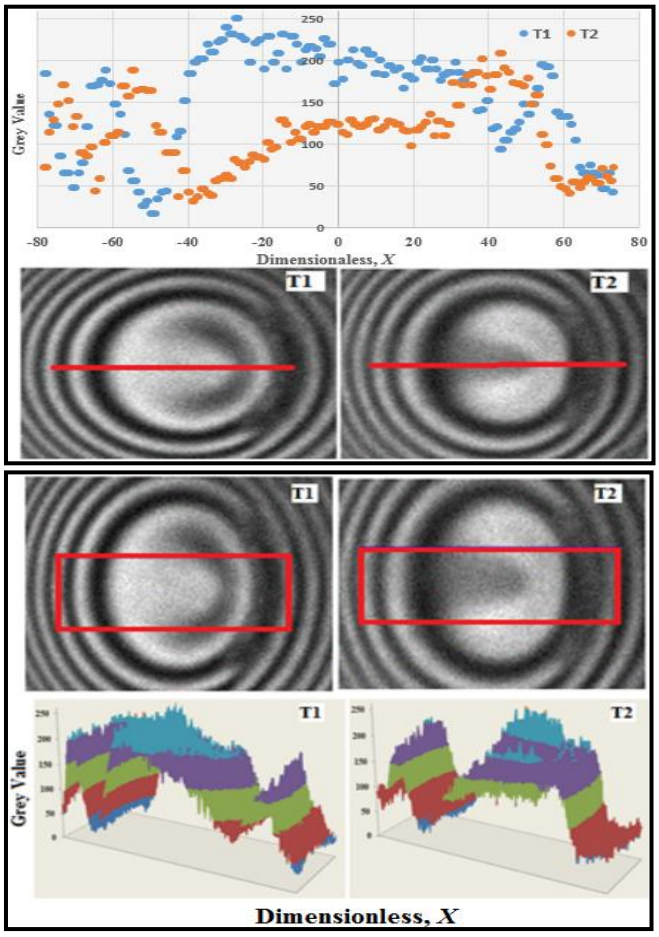

Figure 13 Interferometric images of lubricants film distribution of an EHL point contact operating. *Horizontal 'LINE' and Rectangular 'SLIM' mode.* Parameters: L=2N, U=0.383m/s, T=21°C, P_h=0.205GPa, η for T_1=0.205Pa.s and η for T_2=0.255Pa.s.

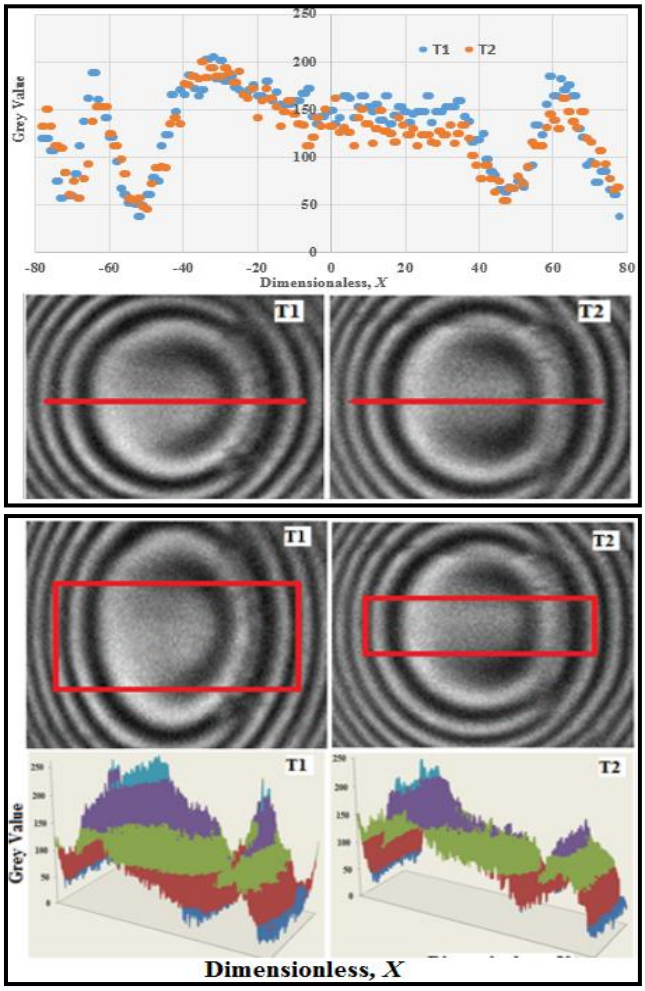

Figure 14 Interferometric images of lubricants film distribution of an EHL point contact operating. *Horizontal 'LINE' and Rectangular 'SLIM' mode.* Parameters: L=2N, U=0.641m/s, T=21ºC, P_h=0.205GPa, η for T_1=0.205Pa.s and η for T_2=0.255Pa.s η.

Load Effect

The influence of load was quickly noted. It was observed that the load differences between loading, markedly affected the even distribution to sustain the film thickness stability. This was observed by the uneven distribution of the film thickness profile both on the *horizontal line* mode and the *rectangular slim* mode in the graphs. There are much sharp peaks observed at high loads than the low loads graphs which indicates sharply the decline of the film thickness [45]. When there is a difference in the mass between moving bodies, the inertia also differs from each other, and therefore, different squeeze speeds are generated at the beginning of impact and the oil entrapment may be different [45]. This obviously influences the film thickness of high loads to decrease sharply. On one hand, blended lubricant, T_2 at the central contact region saw mostly flat surfaces unlike the conventional T_1. On the other hand, the load impact was obvious on all the two lubricants.

Speed Effect

The effect of speed increase is proportional to the increase in the film thickness. All the two tested lubricants proved good for film thickness stability at increase in speed. This is evidenced on the graphs shown in Figure 9 – 14 above, particularly, at high speeds of the blended lubricants T_2. A thick and viscous film under EHL conditions is formed due to the PTFE added to the conventional lubricant. The absence of lubricant improvers in the T_1 led to the poor film thickness stability. Eventually, the grey values of the lubricant become uneven and affect the film thickness of the lubricant. This was clearly observed in all the two lubricants suffering unstable film thickness behavior as shown by the rectangular '*SLIM*' graphs in Figures 9 – 14. But the T_2, which has PTFE additives blended with the base oil, was much firmer than T_1.

PTFE Additive Effect

Finally, the viscosity modifiers [46], PTFE is a good improver and could modify the viscosity of lubricants. The lubricant T_2 happened to have much sharper peaks and very rough on the rectangular *SLIM* mode graphs. This could be attributed to the fact that, the additives were not completely dissolved into oil blending because they are solid powder in nature. The standard lubricant used here was the SAE #30 mechanical oil, but was not able to demonstrate good film thickness stability as the other with PTFE additives.

3.2 Experimental Film Thickness Analysis for ROII Technique

A Matlab computer processing technique was written and used to analyze these pictures to get grey value at desired points or areas. The grey values of the central and minimum contact areas were sampled and used for the calculation. The film thicknesses (h_m and h_c) are then calculated by Equations 4 and 5, the results are shown in bar charts. The tests were conducted at constant 1N and 2N but at varied speeds of 0.189m/s, 0.383m/s and 0.641m/s. The presence of PTFE as a blended additive [46] is adsorbed at the surfaces, increasing the viscosity at the inlet of the contact, resulting in an increase in film thickness at both the central and the minimum film thickness graphs as shown in Figures 15-17 regardless of the load changes.

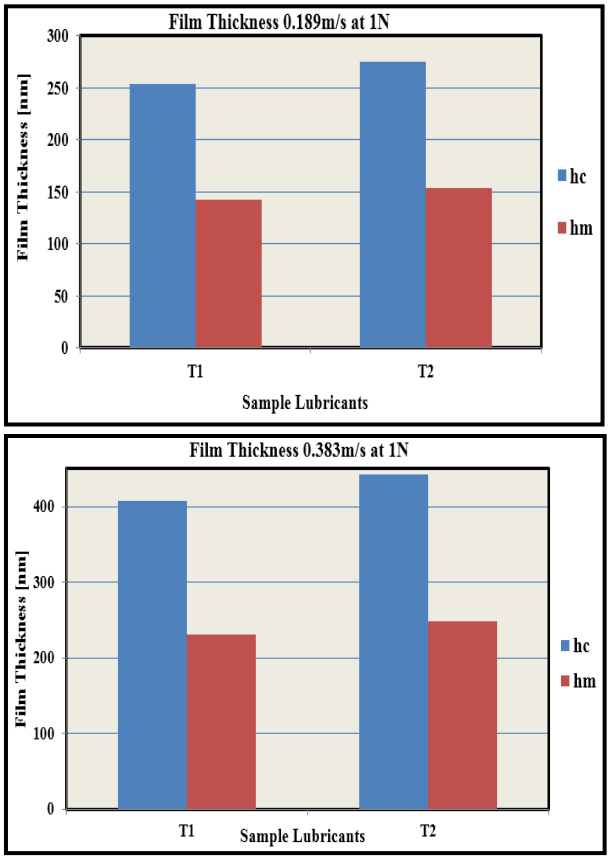

Figure 15 Lubricants experimental film thickness for h_c and h_m, 1N, (0.189m/s, 0.383m/s.)

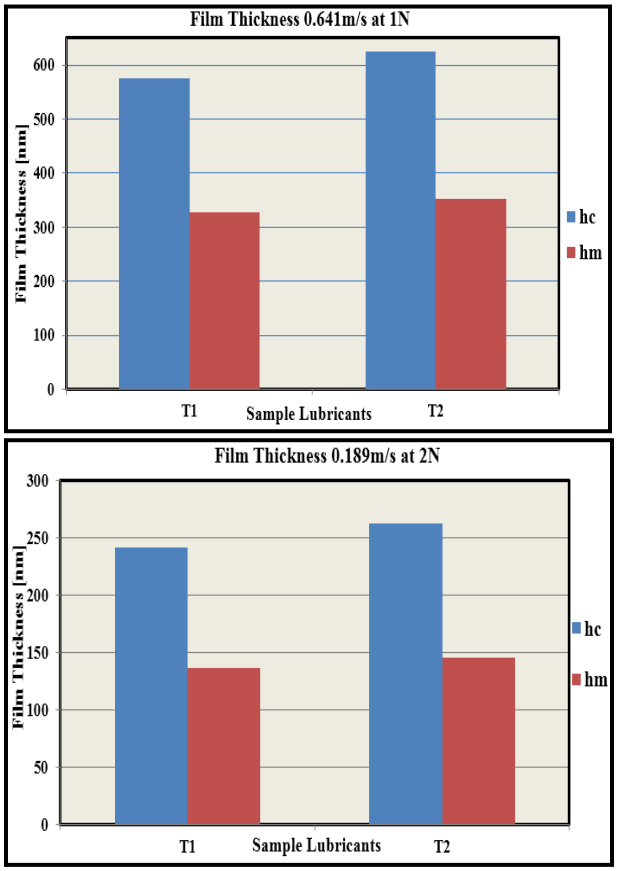

Figure 16 Lubricants experimental film thickness for h_c and h_m, 1N, (0.641m/s, 0.189m/s.)

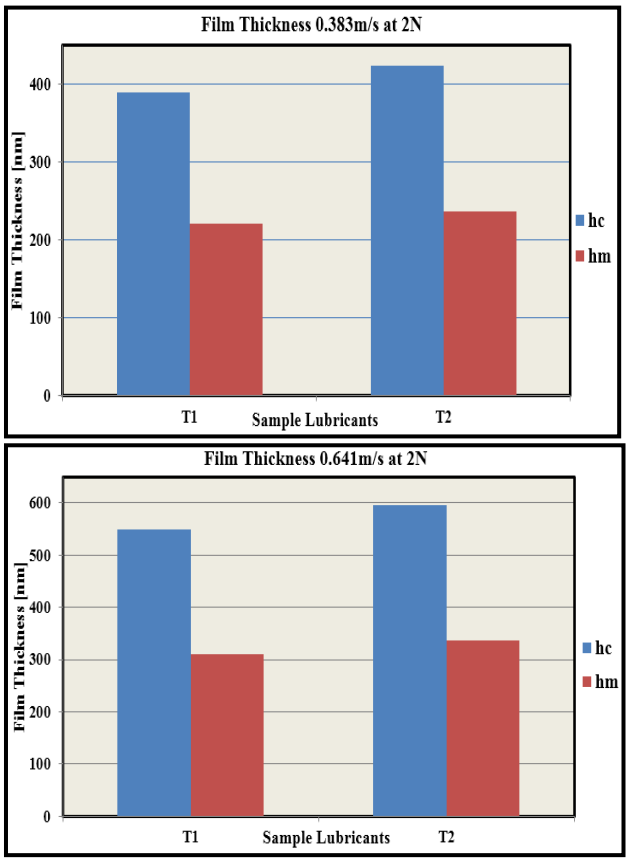

Figure 17 Lubricants experimental film thickness for h_c and h_m, 2N, (0.383m/s, 0.641m/s.)

3.2.1 Film Thickness of Base Lubricant

The EHL Film thickness measurements taken measured for a number of speeds and different load conditions and the resulting graphs are presented in Figures 15-17. The influence of loads on both h_c and h_m are significant. It ranges between (3% to 7%) of film thickness declination. Meanwhile, the speed varies with film thickness of all the lubricants, which led to a great increase in film thickness for both the h_c and h_m at higher speed. On one hand, a clear difference in reduction of film thickness is as a result of load increase. But on the other hand, the film thickness increases with the increase in speed for both the h_c and the h_m. Figures 15–17 give a better understanding of the film thicknesses variation, when measured under constant load but varied speed. Based on the fact that viscosity influences film thickness, it can be concluded that film thickness varies with load and speed. This phenomenon is explained as the contact zone is affected by viscosity thereby, resulting in a lesser film thickness on the T_1 lubricant.

3.2.2 Film Thickness of Liquid – Solid Lubricant

The additive is the PTFE it influences the lubrication process and demonstrated a transitional regime between the

elastohydrodynamic and hydrodynamic lubrication.
Considering the behaviour of the blended lubricants, they behave just as the conventional lubricant. The only difference is that, blended lubricant absorbed surface of the contact increasing the film thickness measurement at both h_c and h_m. As the combination process has been studied thoroughly by previous researchers [47, 48]. Film thicknesses for both the h_c and the h_m of the blended lubricants as T_2 is clearly illustrated in Figures 15–17. With regard to the effect of load, the T_2 blended lubricants suffers film thickness reduction between (2% to 3%) much less and better than T_1 (conventional SAE #30). The speed, as could be seen on the graphs, shows proportional increase in film thickness for both the h_c and h_m for all the sample lubricants tested. Log EHL film thickness as a function of log entrainment speed for fully formulated lubricants. Better still, the T_2 is a much suitable lubricant for sustaining the life of a machine element if further study and proper proportion of the solid lubricants are added.

3.3 Numerical Film Thickness Analysis

The use of the Hamrock and Dowson film thickness Equation 8 and 10, was the numerical method adapted here. The influence of speed and load on fluid film thicknesses at these areas will be the key focus. Instead of the central film thickness, the minimum film thickness has always been of more interest to tribologists, Chaomleffel et al. [49]. Chittenden et al. [49], Hooke [50], and Nijenbanning et al. [51] followed up with different predictions for the central and the minimum film thickness.

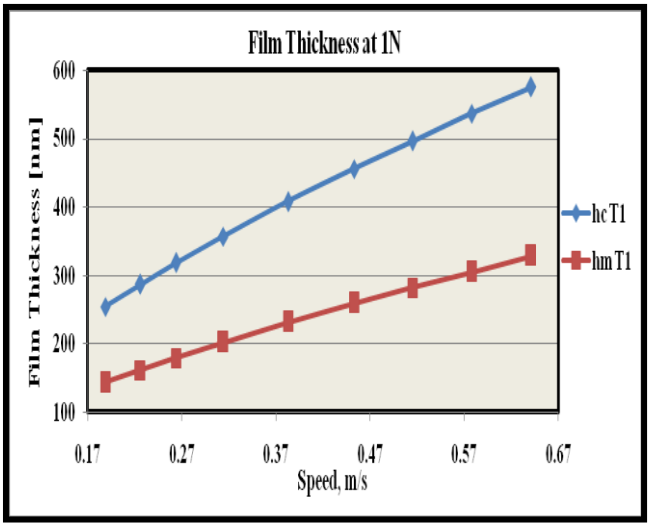

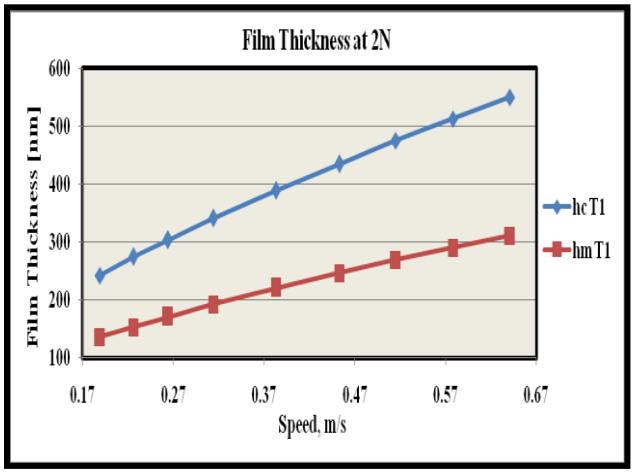

Figure 18 Film thickness as a function of entrainment speed at 1N and 2N (T_1).

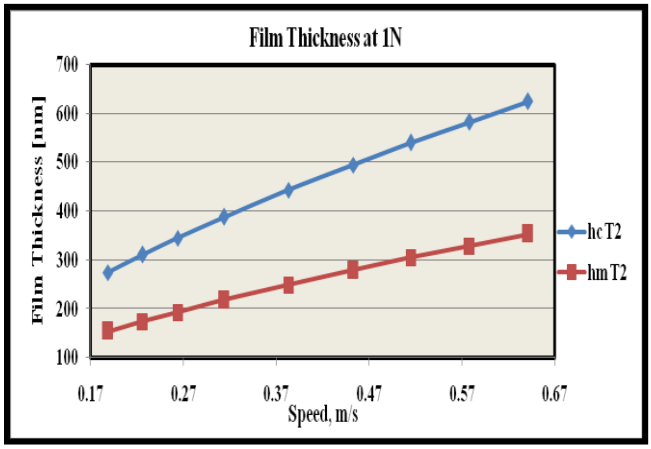

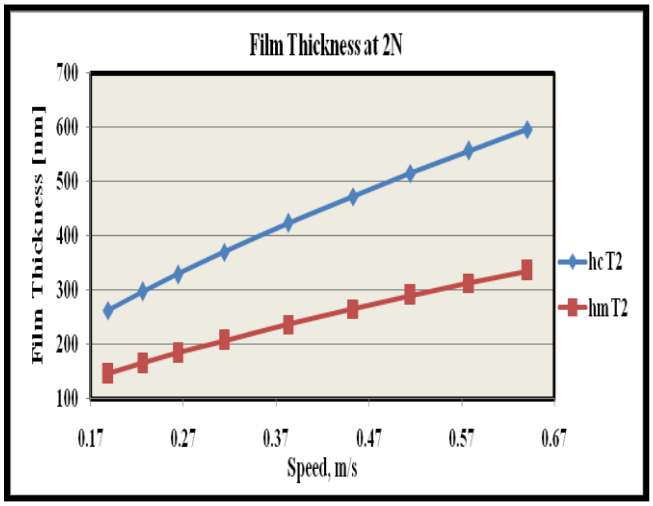

Figure 19: Film thickness as a function of entrainment speed at 1N and 2N (T_2).

However, most approximation formulas have been derived for the central film thickness. The current design uses the Hamrock and Dowson formula, nevertheless, the h_m/h_c ratio factor still holds and depending on the experimental design, based on the film thickness required, thick or thin position, one can determine which range to operate.

3.3.1 Film Thickness of Base Lubricant

The general observation on the base lubricant is that, the film thickness varied with entrainment speed proportionally, yet the film thickness stability could not be sustained, therefore, the film thickness at the exit part suffers high losses and the minimum film thickness is greatly affected. The role of the load can clearly be observed from the graphs as shown in Figure 18. As the load increases at the same speed, the EHL film thickness drops. The drops are not that significant but are a clear indication of film thickness losses of up to about 3% at minimum and 4% at maximum. The lubricant is not able to sustain the film thickness for long due to lack of the ability to stick to the surface of the contacts at entry speed.

3.3.2 Film Thickness of Liquid – Solid Lubricant

The film thickness for the Liquid – Solid lubricants by the Hamrock and Dawson formula conformed to the Venner [37] and Chaomleffel et al. [49] ranges of the h_m/h_c. This is due to the presence of lubricant improvers additives PTFE in the mixture. It has the ability to stick to the surface of the mating part at entry speed and generate film thickness at the restrictive section which is the minimum film thickness section. The entrainment speed could be observed as function of EHL film thickness for lubricant, the T_2 for Figure 19. The T_2 optimized its capacity over the T_1 due to the presence of PTFE. However, they both were in close correlation with their practically obtained results.

3.4 Experimental and Numerical Comparison

The comparison of the experimental film thickness to the Hamrock and Dowson numerically calculated film thickness values were done. As could be seen from the graphs, both results are a function of entrainment speed. The film thickness behaviour increases with increase in the entrainment speed. There is high degree of correlation between the numerically calculated values by the Hamrock and Dawson values and the experimental values.

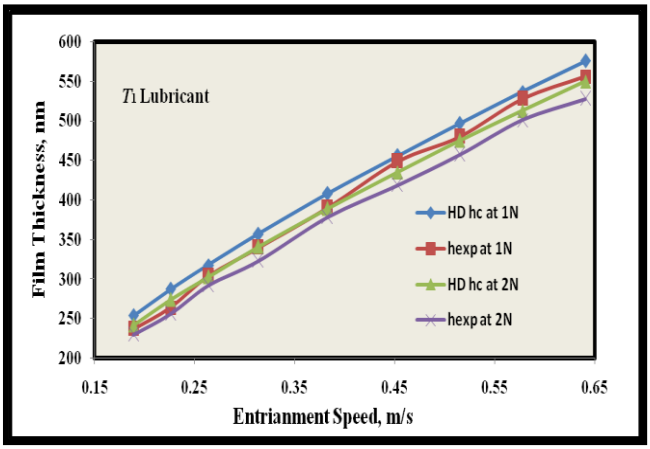

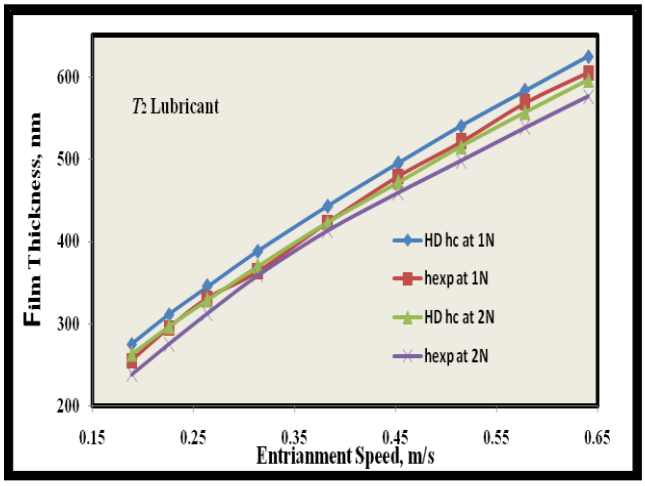

Figure 20 Film Thickness Comparison between Experiment and HD Numerical Calculated (Lubricant T_1 and T_1, Loads are 1N and 2N).

The Figure 20 has two different load results for both the experiment and the numerical methods. The rate of increase of the load is 100% from the first load of 1N to 2N. Nevertheless, the variation of the results of the two are not as high as expected. This might be because of low loads. Therefore, further increase in loads could impact greatly on the film thickness. The polymer additive, PTFE which is included in the SAE #30 is a good lubricant improver agent. It has high resistance to temperature and is able to stabilize the lubricant film thickness for a long time due to its strong molecular bonding. The film thickness is higher than that of the T_1. The film thickness variations of T_2 were found within 200nm to 650nm as compared to the T_1 which was between 200nm and 600nm. The reason for such a difference between the lubricants could be attributed to the additive, whose individual characteristics combined with the SAE #30 lubricant optimize the performance of the blended lubricant T_2. The viscosity of the lubricant is also greatly improved thereby increasing the stability of the film thickness between interfaces. The life span of the machine elements is prolonged due to its better performance. In a nutshell, all the two lubricants were found to have a high correlation at the low loads that was used. The speed generally, varies in direct proportionality to the film thickness. The impact of the viscosity was clear; it controls the stability of the film thickness distribution.

3.5 Theoretical Method Results

In Figure 21 is the ideal illustration of the EHL regime of lubrication under a fully flooded point contact conditions. The dimensionless film thickness, H and the dimensionless pressure, P were obtained in the Figure. The lubricant enters through $-X$ the domain of the profile shown in Figure 21. The film thickness formation could be seen as very even and smooth. In the pressure distribution, it was very smooth

without any sudden change to generate a pressure spike even though the noise in the practical graph. However, this is in a dimensionless situation subject to change in case practical parameters are considered. This program is very practical, friendly, efficient and capable of adapting to changes from the dimensionless film thickness and pressure into dimensional film thickness and pressure. For the load balance to be considered, it is very relevant to adjust the elastohydrodynamic lubrication, h_0 in Equation 11 or H_0 in the Matlab program.

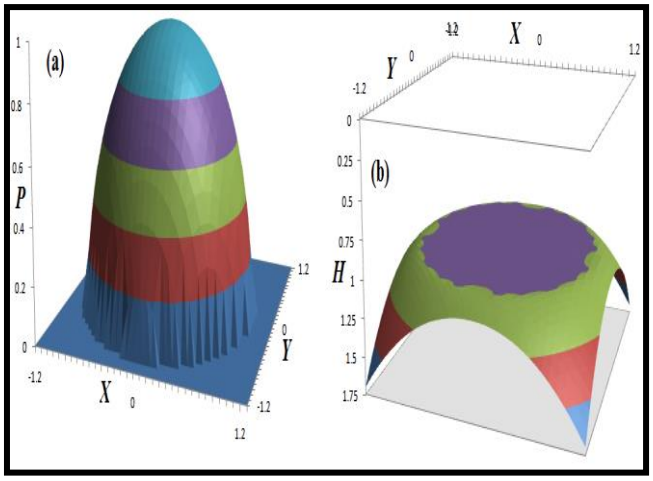

Figure 21 The elastic deformation solution for point EHL contact (a) Pressure distribution *P* and (b) Film thickness *H* after deformation.

3.5.1 Practical Results

The practical values for the relative optical interferometry intensity experiment were used in the program for the sole aim of this work, which was to study the nature of profile between the classical EHL to hydrodynamic in a fully flooded pure rolling point contacts. This regime is most obvious when a system operates in a combination of moderate contact pressures (i.e. moderate piezoviscosity, low normal load, and/or large radii of curvature) and high viscosities, high speeds or low temperatures (i.e. high hydrodynamic effect) applies to nonconformal contacts [52]. Under the EHL conditions given in the program [31], the following results were obtained. These results are purely influenced by the speed and the load of the experimental design. The 'exact parameters' of the practical experiment are computed by using lubricant material properties, geometrical properties of the mating parts and set-up running properties. The Figure 22 – 27 and Figure 28 – 33 are examples of the profiles obtained with the base lubricant and with the PTFE blended with SAE #30 lubricant respectively, operating with low loads 1N and 2N, which were combined with the speeds 0.189m/s, 0.383m/s and 0.641m/s at 21°C room temperature operating condition of the lubricants.

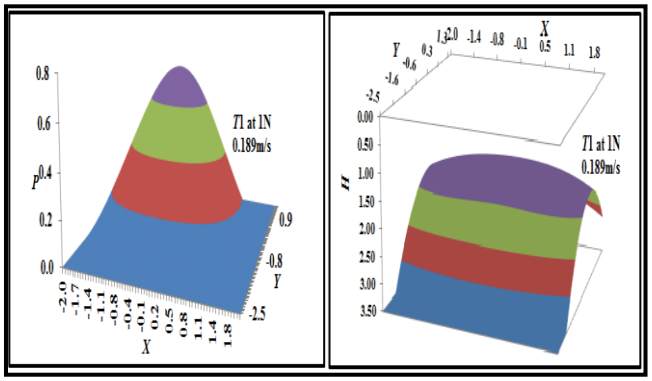

Figure 22 EHL of (H) Film Thickness (P) Pressure Distribution for a constant load (1N) and speed (0.189m/s).

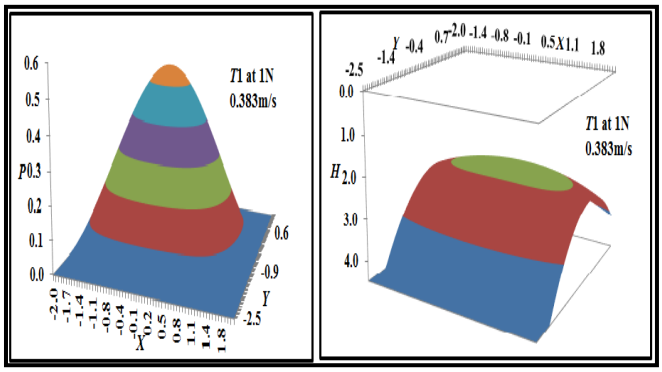

Figure 23 EHL of (H) Film Thickness (P) Pressure Distribution for a constant load (1N) and speed (0.383m/s).

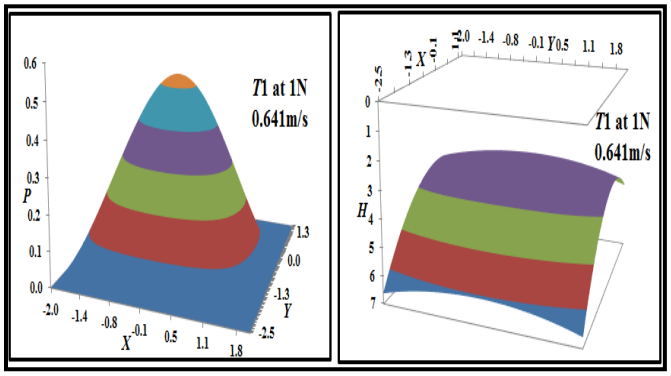

Figure 24 EHL of (H) Film Thickness (P) Pressure Distribution for a constant load (1N) and speed (0.641m/s).

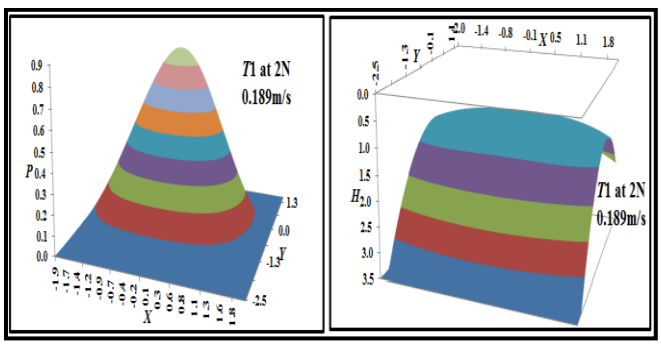

Figure 25 EHL of (H) Film Thickness (P) Pressure Distribution for a constant load (2N) and speed (0.189m/s).

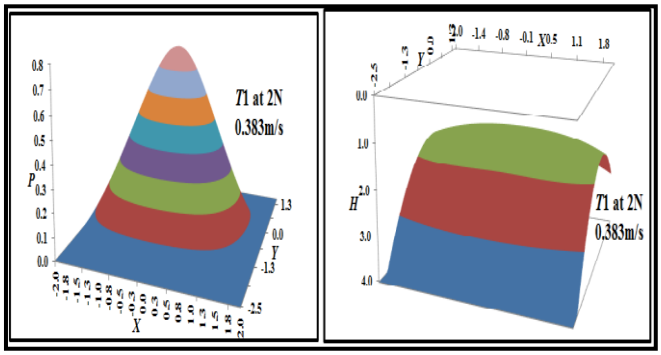

Figure 26 EHL of (H) Film Thickness (P) Pressure Distribution for a constant load (2N) and speed (0.383m/s).

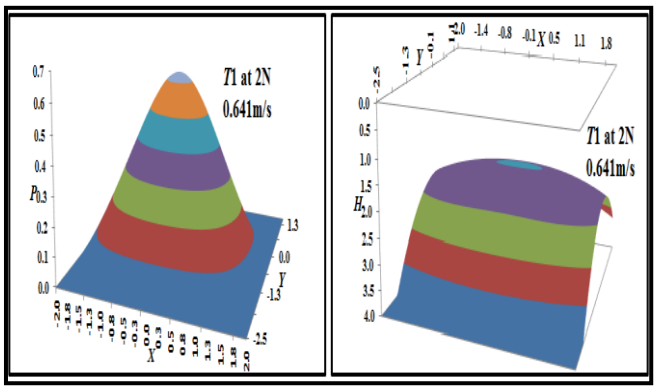

Figure 27 EHL of (H) Film Thickness (P) Pressure Distribution for a constant load (2N) and speed (0.641m/s).

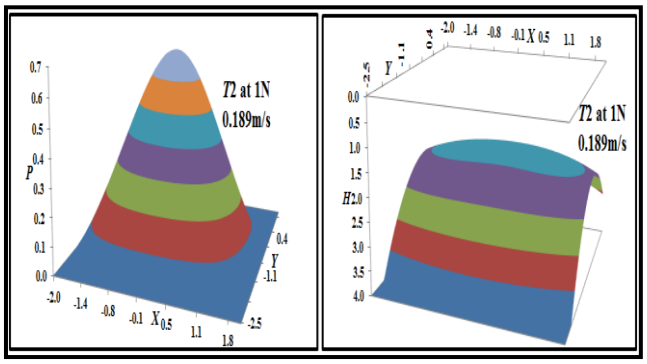

Figure 28 EHL of (H) Film Thickness (P) Pressure Distribution for a constant load (1N) and speed (0.189m/s).

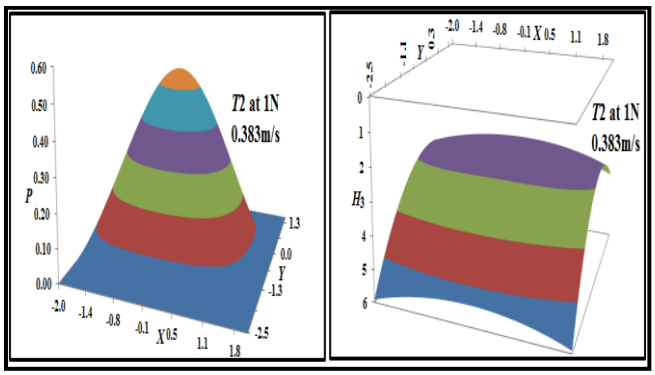

Figure 29 EHL of (H) Film Thickness (P) Pressure Distribution for a constant load (1N) and speed (0.382m/s).

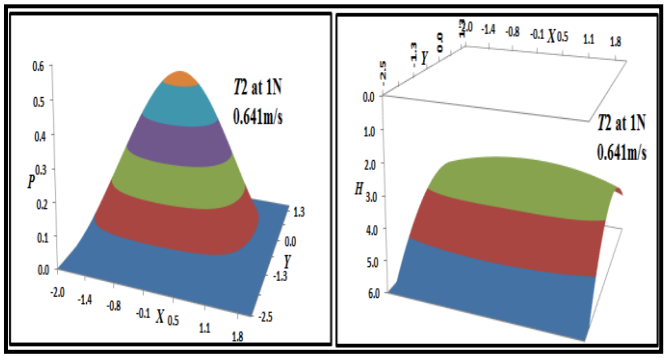

Figure 30 EHL of (H) Film Thickness (P) Pressure Distribution for a constant load (1N) and speed (0.641m/s).

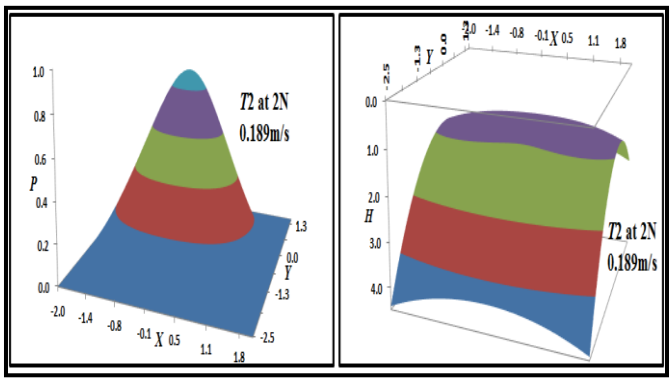

Figure 31 EHL of (H) Film Thickness (P) Pressure Distribution for a constant load (2N) and speed (0.189m/s).

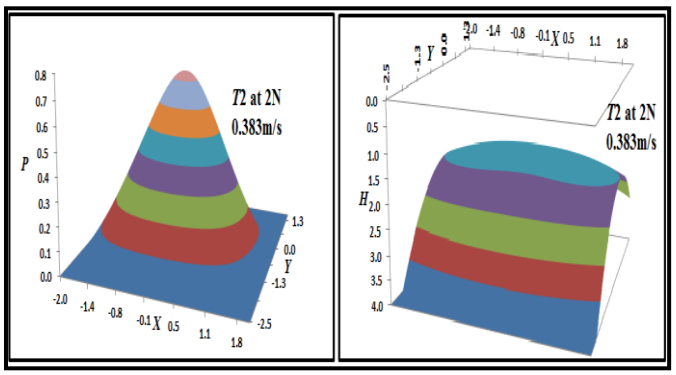

Figure 32 EHL of (H) Film Thickness (P) Pressure Distribution for a constant load (2N) and speed (0.382m/s).

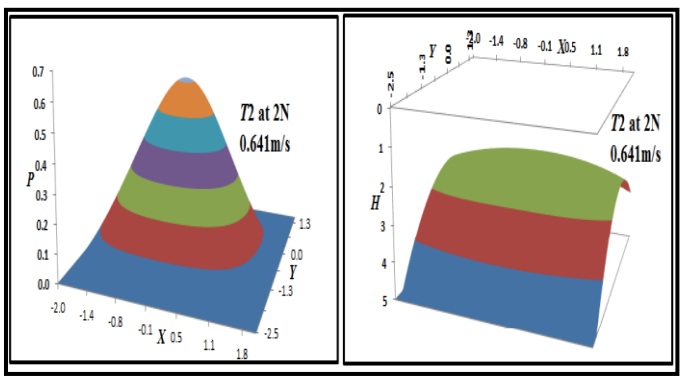

Figure 33 EHL of (H) Film Thickness (P) Pressure Distribution for a constant load (2N) and speed (0.641m/s).

The lubricant enters through the domain at *–X*. At the center of the pressure region, the contact resembles an elliptical Hertzian region. Therefore, even though the experiments were conducted under point or circular contact, it appears to be an elliptical EHL contact. The pressure variation at the boundaries of the Hertzian region is very smooth, there is no abrupt pressure variation to result in pressure (P=0). In view of that, in the outlet or the constriction zone, the local pressure maximum known as the Petrusevich pressure spike [14] did not occur. The film thickness is nearly uniform for almost all the lubricants. But it was very obvious for the blended lubricant with PTFE due to its high viscosity as compared with the base lubricant without any additive. Comparing the obtained results of this study to the classical EHL results by Huang Ping [31], the sample profiles clearly shows a transitional regime between the classical EHL and the hydrodynamic lubrication regimes. This could be attributed to the load and the speed used in this particular study which was the exact parameters used in the practical experimental study and therefore was in line with the prediction of [53] about the transition between the classical EHL and hydrodynamic lubrication regime. The loads used gave a very low maximum Hertz contact pressures as compared to the loads used by Huang Ping [31]. This contributed to the lack of abrupt pressure rise to generate P=0, maximum pressure. The estimated entrainment speeds used for the research work and in running this particular program also contributed to the profiles obtained. The profiles generated for T_1 and T_2 shows the transition between EHL and the hydrodynamic lubrication but not the classical EHL. However, the presence of PTFE additive in the T_2, which is known for high temperature stability, powerful bonding, low coefficient of friction and high resistance to fracture, makes it a much more suitable additive to improve the viscosity, thereby controlling wear and friction between mating parts.

IV. CONCLUSION

The optical technique was used for the experimental analysis and the results compared with other numerical models particularly, the Hamrock and Dawson formula. The conclusion is as follows:

1. The film thickness stability as a function of load, speed and additives were highly confirmed by both the experimental method and the numerical method adopted in these research. The correlation of the obtained values of the experiments and the numerical method, was very high. The graphs for the film thickness stability behavior by horizontal '*LINE'* for all the lubricants conformed to the light intensity variation as a cosine curve [44].
2. The load weakens the film thickness stability of the base oil. But with the inclusion of the PTFE in the T_2 lubricant, the lubricant film thickness stability was improved immensely. This was not the case of the T_1 which is without any additive. The influence of load on the h_m and h_c are significant, it ranges between (3% to 7%) of the film thickness declination.
3. The effect of speed increase is proportional to the increase in the film thickness. At high speeds of the blended lubricants T_2, a thick and viscous film under EHL condition due to the presence of PTFE. The absence of this lubricant improver led to poor film thickness stability of the T_1.
4. The viscosity was a function of pressure, and this had a big influence on the film thickness of the lubricants. The low viscosity lubricant like T_1 had low film thickness values and high viscosity values like T_2 had high film thickness values. The viscosity modifier [42], PTFE is a good improver and could modify the viscosity of the lubricants.
5. Liquid – Solid lubricants can improve and sustain the film thickness stability, thereby prolonging the life span of the machine element, by reducing contact fatigue. The right additive with the right proportion will increase the load carrying capacity of the lubricants and help to decrease the frictional coefficient but increase heat dissipation effect.
6. At the Hertzian contact region, the pressure variation was very smooth. No abrupt pressure variation to result in pressure (P=0). The pressure spike [53] did not occur at the out let section. The loads used in this research work, gave a very low maximum Hertz contact pressures than the loads used by Prof. Huang Ping [31]. Due to the operating parameters used for this study, the overall observation of the results exhibits a transitional regime between the classical EHL and the hydrodynamic lubrication regime.

ACKNOWLEDGMENT

This work was supported by the National Natural Science Foundation of China (Grant No: 51575190, 51675105 and 51575113) and China Post-Doctoral Fund (Grant No: 2015M582357). Special gratitude to the Special Support Fund of Guangdong Province (2014TQ01X542) and Fundamental Research Funds for Central Universities (2015ZZ080) for supporting this work.

REFERENCES

[1] Sivayogan, G.; Rahmani, R.; Rahnejat, H. Lubricated loaded tooth contact analysis and non-Newtonian thermoelastohydrodynamics of high-performance spur gear transmission systems. Lubricants 2020, 8, 20.

[2] Glenn K. G., (2014) "Study of TEHL Point Contact Lubricated With Two-Phase (Liquid-Solid) Lubricants" Ph.D. Dissertation, South China University of Technology, Guangzhou, China.

[3] Bercea, M., Bercea, I., Nelias, D. and Olaru, D.N., (1999a), "Polyethylene as an Additive for Mineral Oils - Pan I: Influence of the Polymer Concentration on the

Film-Forming Properties in Rolling Bearing," Trib. Trans., 42. pp 851-859.

[4] Cann, P. C. and Spikes, H. A., (1994), "The Behavior of Polymer Solutions in Concentrated Contacts: Immobile Surface Layer Formation," Trib. Trans., 37, pp 580-586.

[5] Georges, E., Georges, J. M. and Diraison, C., (1996), "Rheology of Olefinic Copolymer Layers Adsorbed on Solid Surfaces," Trib. Trans, 39, pp 563-570.

[6] Hayashi, H., (1991). "Recent Studies on Fluid Film Lubrication with Non-Newtonian Lubricants," Japan Soc. Mech. Eng., 34, pp 1 - 11.

[7] Mitsui, H. and Spikes, H. A,, (1998). "Predicting EHD Film Thickness of Lubricant Polymer Solutions," Trib. Tvaru. 41, pp 1-10.

[8] Smeeth, M., Spikes, H. A. and Gunsel, S., (1996), "Performance of Viscosity Index Improvers in Lubricated Contacts." Langmuir, 12, pp 4594-4598.

[9] S.A. Mohamed, N.S. Ahmed, S.M. Hassanein, A.M. Rashad, Investigation of polyacrylates copolymers as lube oil viscosity index improvers, J. Petrol. Sci. Eng. 100 (2012) 173–177.

[10] Spikes. H. A., Cann, P. M.. Coy. R. C. and Wardle. R. W. N.. (1990) "An 'In Lubro' Study of VI Improvers in EHD Contacts," Lubc Sci., 3, pp 45-62,.

[11] W.B. Jez, A.S. Braga, S.M. Ingrid, Determination of viscosity index in lubricant oils by infrared spectroscopy and PLSR, Fuel 120 (2014) 171–178.

[12] Kaneta, M.; Ogata, T.; Takubo, Y.; Naka, M. Effects of a thickener structure on grease elastohydrodynamic lubrication films. Proc. Inst. Mech. Eng. J 2000, 214, 327–336, doi:10.1243/1350650001543214.

[13] Omneis, J.. Nevdorfl. P. and Pennewi P. H.. (1993) "Mixed Polymers-An Effective Solution for the Blending Plant," in Pmc. 6th Int'l. Congress on Trib... EUROTRlB' 93 (Budapest). 5. pp 4 10-4 15..

[14] Hirano. F., Kuwano. N. and Ohno. N., (1980) "Effect of Molecular Weight Distribution of Mineral Oils on Life of Thrust Ball Bearings." ASLE Trans. 26, pp 545-552..

[15] Larsson, P.O.; Larsson, R.; Jolkin, A.; Marklund, O. Pressure fluctuations as grease soaps pass through an EHL contact. Tribol. Int. 2000, 34, 211–216, doi:10.1016/S0301-679X(00)00033-

[16] A. Martini, U. S. Ramasamy, M. Len, (2018), "Review of Viscosity Modifier Lubricant Additives" Tribology Letters, https://doi.org/10.1007/s11249-018-1007-0.

[17] Smeeth. M. Spikes. H. A. and Gunsel. S., (1996) 'The Formation of Viscous Surface Films by Polymer Solutions: Boundary or Elastohydrodynamic Lubrication?" Trib. Trans., 39, pp 720-725,.

[18] Smeeth. M. Spikes, H. A. and Gunsel. S., (1996) "Boundary Film Formation by Viscosity Index Improvers," Trib. Trans., 39, pp 726-734,.

[19] H. Spikes, Tribol Lett, (2015), "Friction Modifier Additives" Article number: 5, 60.

[20] J. Guegan, M. Southby, H. Spikes, (2019), "Friction Modifier Additives, Synergies and Antagonisms", Tribology Letters, 67:83.

[21] Dowson, D. (1999), History of Tribology, John Wiley & Sons: New York.

[22] Pitenis, A.A., Ewin, J.J., Harris, K.L., Sawyer, W.G., Krick, B. A.: (2014) "In vacuo tribological behavior of polytetrafluoroethylene (PTFE) and alumina nanocomposites: the importance of water for ultralow wear." Tribol. Lett. 53, 189–197.

[23] Kucu komeroglu, T., Kara, L.: (2014) "The friction and wear properties of CuZn39Pb3 alloys under atmospheric and vacuum conditions." Wear 309, 21–28.

[24] Tagawa, M., Ikeda, J., Kinoshita, H., Umeno, M., Ohmae, N.: (2001) "Effect of atomic oxygen exposures on the tribological properties of molybdenum disulfide lubricants." In: Kleiman, J., Tennyson, R. (eds.) Protection of Space Materials from the Space Environment, pp. 73–84. Springer, Netherlands.

[25] Field, S.K., Jarratt, M., Teer, D.G.: (2004) "Tribological properties of graphite-like and diamond-like carbon coatings." Tribol. Int. 37, 949–956.

[26] Liu, B.X., Pei, X.Q., Wang, Q.H., Sun, X.J., Wang, T.M.: (2012) "Structural and tribological properties of polyimide /Al2O3/SiO2 composites in atomic oxygen environment." J. Macromol. Sci. Phys. 51, 224–234.

[27] Kiefer, R.L., Gabler, W.J., Hovey, M.T., Thibeault, S.A.: (2011) "The effects of exposure in space on two high-performance polymers". Radiat. Phys. Chem. 80, 126–129.

[28] Agag, T., Koga, T., Takeichi, T.: (2001) "Studies on thermal and mechanical properties of polyimide–clay nanocomposites". Polymer 42, 3399–3408.

[29] Zafarani, H.R., Abdi, M., Bahrololoom, M.E.: (2014) "Wear behavior of PTFE hydroxyapatite composite fabricated by hot-press sintering process." Acta Metall. Sin. 27, 347–351.

[30] Selby, T. W., (1958) "The Non-Newtonian Characteristics of Lubricating Oils," ASIX Trans., 1, pp 68-81,.

[31] Huang P., (June, 2012) "Lubrication Numerical Calculation Methods", Published by Higher Education Press, Beijing, P. R. China.

[32] Luo, J.B., Wen, S.Z., Huang, P.: (1996) "Thin film lubrication, part I: the transition between EHL and thin film lubrication." Wear 194, 107–115.

[33] Luo, J.B., Wen, S.Z.: (1996) "Mechanism and characteristics of thin film lubrication at nanometer scale" Sci. China Ser. A 39(12), 1312–1322.

[34] R. R. Bommareddi, (2014), "Application of Optical Interferometer Techniques for Percision Measurement of Changes in Temperature, Growth and Refractive Index of Materials." Technologies, 2, 54-75.

[35] M. Born and E. Wolf, (1975), "Principle of Optics", 5th Edition, Pergamon Press, pp. 257-270.

[36] Moes, H. (2000), "Lubrication and Beyond", Lecture Notes, Code 115531, Twente University Press, Enschede, Netherlands, 366 p.

[37] Venner, C.H. (1991), "Multilevel solution of the EHL line and point contact problems", Ph.D. Dissertation, Twente University, Netherlands, 318 pp.

[38] Hooke, C.J., (1988) "Minimum film thickness in lubricated point contacts operating in the elastic piezoviscous regime", Proc. IMechE, Part C: J. Mech. Engineering Sc., 202 (C2), 73–84.

[39] M. Marian, M. Bartz, S. Wartzack and A. Rosenkranz, (2020), "Non-Dimensional Groups, Film Thickness Equations and Correction Factors for Elastohydrodynamic Lubrication: A Review", Lubricants, 2020, 8, 95; doi:10.3390/lubricants8100095.

[40] Hamrock, B. J., and Dowson, D., (April 1976) "Isothermal Elastohydrodynamic Lubrication of Point Contacts: Part 1 - Theoretical Formulation", Trans. ASME Journal of Lubrication Technology 98 223.

[41] Hamrock, B. J., and Dowson, D., (July 1976) "Isothermal Elastohydrodynamic Lubrication of Point Contacts: Part 2 - Ellipticity Parameter Results", Trans. ASME, Journal of Lubrication Technology 98 375.

[42] Hamrock, 13. J., and Dowson, D., "Isothermal Elastohydrodynamic Lubrication of Point Contacts: Part 3 - Fully Flooded Results", Trans. ASME, Journal of Lubrication Technology 99 (April 1977) 264.

[43] Hamrock, B. J., and Dowson, D., (1977) "Isothermal Elastohydrodynamic Lubrication of Point Contacts: Part 4- Starvation Results", Trans. ASME, Journal of Lubrication Technology 99 15.

[44] Ma L. R., Zhang C. H., (2009) "Discussion on the Technique of Relative Optical Interference Intensity for the Measurement of Lubricant Film Thickness" Tribol Lett. 36:239-245.

[45] Dumitru M. F.,(2011) Study of Film Formation in EHD Contacts Using a Novel Method Based on Electrical

Capacitance, Submitted for the degree of Doctor of Philosophy, Department of Mechanical Engineering, Brunel University.

[46] Westlake, F. J. and Cameron, A. (1967-8) "A study of ultra-thin lubricant film using an optical technique." Proc. Instn. Mech. Engrs., 182(3G), 75-78.

[47] M. Smeeth, H. A. Spikes, S. Gunsel (1996) "The Formation of Viscous Surface Films by Polymer Solutions: Boundary or Elastohydrodynamic Lubrication" TribologyTransactions, Vol. 39, 726–734.

[48] M. Smeeth, H. A. Spikes, S. Gunsel (1996) "Boundary Film Formation by Viscosity Index Improvers" Tribology Transactions, Vol. 39, 726–734.

[49] Chaomleffel, J.-P., Dalmaz, G., and Vergne, P. (2007) "Experimental results and analytical film thickness predictions in EHD rolling point contacts" Tribol. Int., 40(10-12, Special Issue), 1543-1552.

[50] Hooke, C. J. (1990) "An interpolation procedure for the minimum film thickness in point contacts." Proc. IMechE, Part C: J. Mechanical Engineering Science, 204, 199–206.

[51] Nijenbanning, G., Venner, C. H., and Moes, H. (1994) "Film thickness in elastohydrodynamically lubricated elliptic contacts." Wear, 176, 217–229.

[52] G. Dalmaz, J-P Chaomleffel and P. Vergne, (May, 2009) "An exploration of the elastohydrodynamic – hydrodynamic transition through film thickness measurements in rolling point contacts" Proceedings of the IMechE; part J., Journal of Engineering Tribology, 223:529.

[53] Petrusevich A.I. (1951) 'Fundamental conclusions from the contact-hydrodynamic theory of lubrication.' Izv. Akad. Nauk. SSSR (OTN), Vol 2, p. 209.